Wireless Measurement of Float-Sink Motion of Variously-shaped Objects in Gas-Solid Fluidized Bed

Koshi Uemoto [a], Shohei Narita [a], Shusaku Harada [a,*],
Yuya Sakamoto [b], Takuya Tsuji [b], Jun Oshitani [c],
Hirokazu Kajiwara [d] and Kei Matsuoka [e]

[a] Department of Mechanical Engineering, Osaka University, 2-1 Yamada-oka, Suita, Osaka 565-0871, Japan

[b] Division of Sustainable Resources Engineering, Faculty of Engineering, Hokkaido University, N13-W8 Sapporo, Hokkaido 060-8628, Japan

[c] Department of Applied Chemistry, Okayama University of Science, 1-1 Ridai-cho, Kita-ku, Okayama 700-0005, Japan

[d] Ebara Environmental Plant Co., LTD., 11-1 Haneda Asahi-cho, Ota-ku, Tokyo 144-0042, Japan

[e] Ebara Corporation, 11-1 Haneda Asahi-cho, Ota-ku, Tokyo 144-8510, Japan

* Corresponding author: Shusaku Harada
Phone/Fax: + (81)-11-7066310
E-mail address: harada@eng.hokudai.ac.jp

ABSTRACT

The float-sink motions of coarse objects in a gas-solid fluidized bed were investigated experimentally using a newly developed wireless sensor system. The Lagrangian sensor system developed by our previous study, which can measure the vertical position of a freely-moving object in an invisible system, was extended to measure the attitude angle and vertical position of variously-shaped objects simultaneously. The vertical motion of objects with the same mass and volume but different shapes was measured using the Lagrangian sensor under density conditions similar to the apparent density of the fluidized bed. The results demonstrate that the float-sink motions of objects in the gas-solid fluidized bed differ significantly depending on the shape of the object, even at the same density, in contrast to those in water. It was found that non-spherical objects tend to float more easily than spherical objects, which supports the numerical results shown in our previous study (Tsuji et al., Chem. Eng. Sci., 2022). Simultaneous measurement of the position and attitude angle highlights the importance of the angular motion of objects in terms of the float-sink motion. The interaction of the object with the media particles in the fluidized bed differs depending on the object shape, which indicates that each shape involves a unique float-sink mechanism.

Keywords: Fluidized bed, Wireless measurement, Floating and sinking, Non-sphericity, Attitude angle

1. Introduction

Solid objects immersed in a gas-solid fluidized bed exhibit a wide variety of motions depending on their sizes and shapes. Some of these motions are similar to those in liquids, e.g., a buoyant motion [1,2], while others, e.g., unexpected circulation and segregation, cannot be observed in liquids [3-5]. These phenomena in a fluidized bed are important in various engineering processes such as biomass combustion [6,7] and dry density separation [8]. In case of a large size difference between the immersed object and media particles of the fluidized bed, various anomalous motions can occur, at least within the framework of fluid mechanics or other continuum mechanics [9, 10] To the best of our knowledge, these mechanisms have not yet been understood.

In particular, objects immersed in a bubbling fluidized bed exhibit complex behavior depending on air velocity and as well as the object density. Many experimental and numerical studies have been conducted on such systems, and recent studies attempts to measure object motion in a fluidized bed using non-invasive techniques, e.g., XPIV (X-ray particle image velocimetry) [4,5], MRI (magnetic resonance imaging) [11], RPT (radioactive particle tracking) [3,12], MPT (Magnetic particle tracking) [13], PEPT (positron emission particle tracking) [14]. In similar attempts, Lagrangian measurement systems using MEMS sensors, which can measure physical quantities from the Lagrangian point of view (following its motion), have been developed in the field of multiphase flow dynamics [15-21]. In the previous studies, we examined the motion of coarse objects in a gas-solid fluidized beds using Lagrangian sensors, which can wirelessly measure the position and the force acting on freely moving objects in granular media, that cannot be observed from the outside [22, 23].

Higashida et al. utilized a Lagrangian sensor to measure the force acting on an object in a gas-solid fluidized bed and compared the measurement results with the numerical results under the same conditions [22]. In addition, Yoshimori et al. modified the Lagrangian sensor to measure the vertical position and force simultaneously, and they applied it to the motion of a spherical object in a fluidized bed [23].

These previous studies revealed that the float-sink motion in a fluidized bed exhibit similarities and dissimilarities with those in a liquid. Ideally, a uniform pressure gradient is formed in the fluidized bed due to air permeation flow, which is balanced by the mass of the media particles. This pressure gradient acts like a hydrostatic pressure, and the object is subjected to buoyancy that is proportional to the apparent density of the fluidized bed. However, the previous studies by the Lagrangian measurements and numerical analyses showed that the float-sink motion in a fluidized bed depends on the fluidization state of the bed complicatedly [23,24].

In this study, we focused on the effect of the object shape on its float-sink motion in the fluidized bed. Within the framework of fluid mechanics, the vertical motion of the object should be determined entirely by its density, independent of its shape. However, the object motion in the fluidized bed is also affected by the local fluidization state of the media particles around it, in addition to the background pressure field. Recently, we performed some studies from this perspective, i.e., numerical simulations of the motion of non-spherical objects in a fluidized bed using a new numerical scheme [25], and direct measurements of fluid forces acting on non-spherical objects fixed in a fluidized bed [26]. These results demonstrated that the object shape influences both the local motion of media particles and the air flow adjacent to the object.

The present study is coupled with our recent study on numerical simulations of non-spherical objects in gas-solid fluidized beds [25]. Under the same conditions as the numerical simulation, experiments were conducted using a new Lagrangian sensor system. We developed the existing sensor system for the simultaneous measurement of the vertical position and force [23] to realize non-invasive measurement of the attitude angle of the object. The measurement of attitude angle can help us understand the angular motion of non-spherical objects in a fluidized bed, which cannot be observed externally. In this study, we focused on the details of the experimental method and the results on the detailed motion of non-spherical objects that were not presented in the previous study [25].

2. Experimental Method

2.1 Wireless Sensor System

A wireless sensor system was used to measure both the vertical position and attitude angle of non-spherical objects in a gas-solid fluidized bed, which cannot be observed directly. In the previous researches, we developed a Lagrangian sensor system to wirelessly measure its own position and the force acting on itself in liquid [19], and in a gas-solid fluidized bed [22,23]. In this study, a new sensor system for the simultaneous measurement of the vertical position and attitude angle of non-spherical objects, which moves freely, was developed based on the existing Lagrangian sensor as reported in the previous studies.

Figure 1 shows the circuit diagram and outer appearance of the newly developed Lagrangian sensor, which includes a built-in 9-axis motion sensor (3-axis acceleration sensor, 3-axis magnetometer and 3-axis gyroscope), a signal processor, a wireless transmitter, and cells. Note that the motion sensor (InvenSense, MPU9250) in the new system is the same as that used in the previous version [23], however, a new signal processor (Vitro, 8pino) is introduced. 8pino is an Arduino compatible device that can be mounted in a very small space (23.5 mm × 8 mm × 0.8 mm). The analog signals obtained by the built-in sensors are converted into multiple 8-bit digital signals and serialized via USART in the 8pino. The serialized signals are then sent via the wireless transmitter (433MHz) to the receiving module connected to a personal computer non-invasively. The set of measured data is obtained every 62.5 ms. As reported our the previous study, the vertical position and the force acting on the object can be measured simultaneously using our Lagrangian sensor system [23]. In this study, the attitude angle of non-spherical objects was also detected from the output signals. Here we focused on the relationship between the float-sink motion and the attitude of object and therefore this study did not address the force acting on the object. The details of the measurement principles are given in a later section.

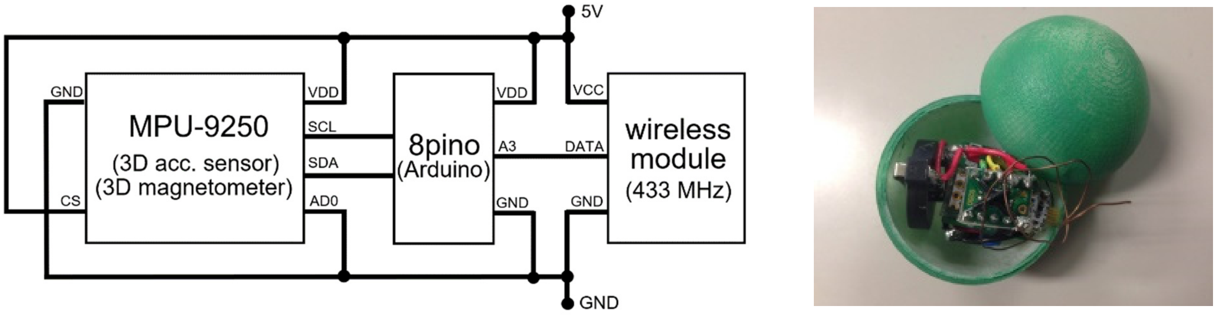

(a) circuit diagram (b) appearance

Fig.1 Wireless measurement system of object motion.

2.2 Fabrication of variously-shaped sensors

The non-spherical objects were designed based on the super-ellipsoid model, which describes the transition from spherical to non-spherical shapes arbitrarily [27]. In this model, the object shape can be obtained by the following equation.

$$F(x) = \left(\left| \frac{x_1}{r_1} \right|^{2/\varepsilon_1} + \left| \frac{x_2}{r_2} \right|^{2/\varepsilon_1} \right)^{\varepsilon_1/\varepsilon_2} + \left| \frac{x_3}{r_3} \right|^{2/\varepsilon_2} \tag{1}$$

where x_1, x_2 and x_3 represent the Cartesian coordinates, r_1, r_2 and r_3 are constants that describe the aspect ratio of the object in each direction, and ϵ_1 and ϵ_2 are constants that describe the corner shape of the object. Our research group has performed numerical analyses of the object motion in a gas-solid fluidized bed, and experiments of pressure measurements around a fixed object in a fluidized bed under the assumption of the same object geometry. The detailed explanation and parameter setting of the super-ellipsoid model can be found in the previous studies [25,26].

The outer shellsof the Lagrangian sensor were fabricated using a 3D printer. The upper images of Fig.2 show the shapes of the non-spherical objects considered in this study. The disk-shaped objects with aspect ratios (the ratio of the longest to the shortest length) of $Ar = 2$ and $Ar = 3$, the spherical object, and the cylindrical objects with $Ar = 2$ and $Ar = 3$ were designed based on the super-ellipsoid model. Note that the diameter of the spherical object is 40 mm. In addition, the short and long lengths of the disk ($Ar = 3$) are 17.9 mm and 52.5 mm, respectively. Similarly, the short and long lengths of the cylinder ($Ar = 3$) are 25.6 mm and 75.6 mm, respectively. All considered objects have the same volume $V = 33.5\times10^3$ mm^3, thus, only the effect of the object shape on the float-sink motion can be considered. The lower images of Fig.2 show images of the actual sensor inside the fabricated capsules.

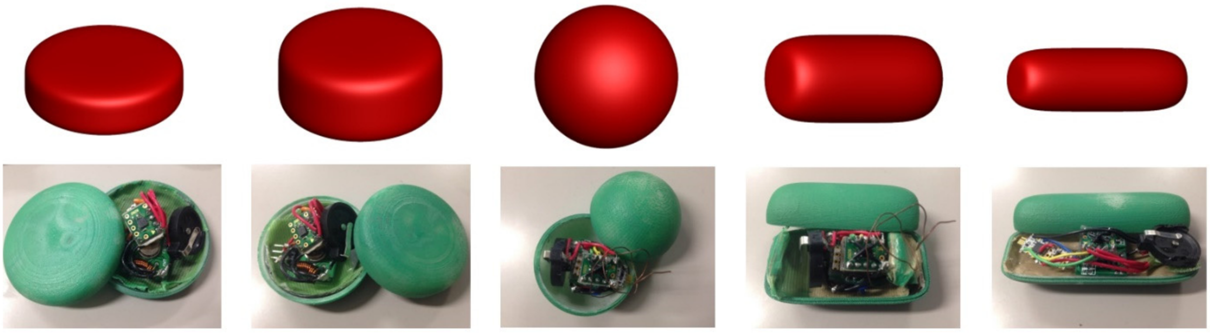

(a) disk (Ar=3) (b) disk (Ar=2) (c) sphere (d) cylinder (Ar=2) (e) cylinder (Ar=3)

Fig.2 Outer appearance of variously-shaped capsules with built-in wireless sensor system.

Since the inner spaces of non-spherical objects are distorted, each component of the sensor system was constructed separately. Therefore, we cannot adjust the center of gravity accurately with the present sensor system. In addition, the motion sensor cannot be positioned precisely at the center of the capsule due to the limitations of the inner space. Consequently, the accuracy of positional measurement in the present system is inferior to the sytem used in the previous study [23], with a maximum error of approximately 20 mm.

2.3 Measurement Principles

Figure 3 shows the measurement principles of the Lagrangian sensor system to acquire the vertical position and attitude angle. The principle of vertical position measurement was described in detail in the previous study [23] and therefore this section only provides a concise overview. The measurement system consists of the Lagrangian sensor system built into capsules of various shapes, the receiving module connected to a personal computer, and a pair of coils (Maxwell coil) installed outside (also see Fig.4). As shown in Fig. 3, the Maxwell coil generates linear magnetic fields of different magnitudes in the axial (vertical) direction. The magnetic sensor built in the capsule measures the magnetic vector at each position and the transmitter transmits the signals wirelessly to the outside. The lower half region between two coils was used as the measurement. By preparing the calibration curve of the relationship between the vertical position and magnetic intensity, the vertical position of the object (i.e., Lagrangian sensor) at each instant of time can be detected. The precision of the positional measurement is described in detail in our previous study [23].

In this study, the attitude angle of a non-spherical object relative to the vertical direction was also acquired from the magnetometer output. The 3 axis magnetometer detects the component of the magnetic vector in sensor-fixed coordinates $\tilde{\boldsymbol{b}} = (\widetilde{b_x}, \widetilde{b_y}, \widetilde{b_z})$. As shown in Fig.3, the definition of the attitude angle differs depending on the object shape. For example, with disk-shaped object, the attitude angle θ_z is defined as the angle between the vertical direction and the direction of the normal vector of the disk surface (i.e., z axis in sensor fixed coordinates) as follows.

$$\cos\theta_z = \frac{\widetilde{b_z}}{\sqrt{\widetilde{b_x}^2 + \widetilde{b_y}^2 + \widetilde{b_z}^2}} \tag{2}$$

For the cylinder-shaped objects, the attitude angle θ_x is defined as the angle between the vertical direction and the direction of the long-side direction of the cylinder (i.e., x axis in sensor fixed coordinates) as follows.

$$\cos\theta_x = \frac{\widetilde{b_x}}{\sqrt{\widetilde{b_x}^2 + \widetilde{b_y}^2 + \widetilde{b_z}^2}} \tag{3}$$

From the above equations, the attitude of non-spherical objects at each instant of time can be obtained from the measured results of the magnetic vector.

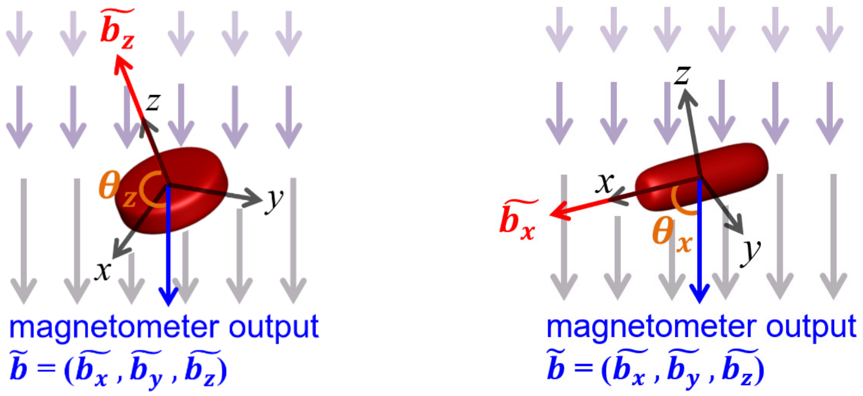

(a) disk (b) cylinder

Fig.3 Principle of vertical position and attitude angle measurements.

2.4 Experimental Setup

Figure 4 shows a schematic diagram of the experimental system. The experimental apparatus of a gas-solid fluidized bed has a rectangular cross section of 150mm×150mm. The apparatus of the fluidized bed is connected to an air-inlet system via a distributor made of SUS mesh films, sponges, and filter cloths. The Maxwell coil system is set around the fluidized bed. The height of the lower coil equal to the height of the bottom of the fluidized region.

The experimental conditions in this study was essentially the same as those of the numerical simulation conducted in our previous study [25]. The media particles were glass beads of diameter d_p = 600–850 μm and density ρ_p = 2500 kg/m^3 (B-type particles in Geldart classification [28]). The inlet air velocity u_0 was controlled using a mass flow controller based on the minimum fluidization velocity u_{mf}. In this study, the inlet velocity was fixed at u_0/u_{mf} = 4.0. The fluidization state of media particles in such a condition corresponds to the bubbling fluidization state, which is a typical state of Geldart B particles, as can be referred in the previous study [23]. Under this air velocity condition, a

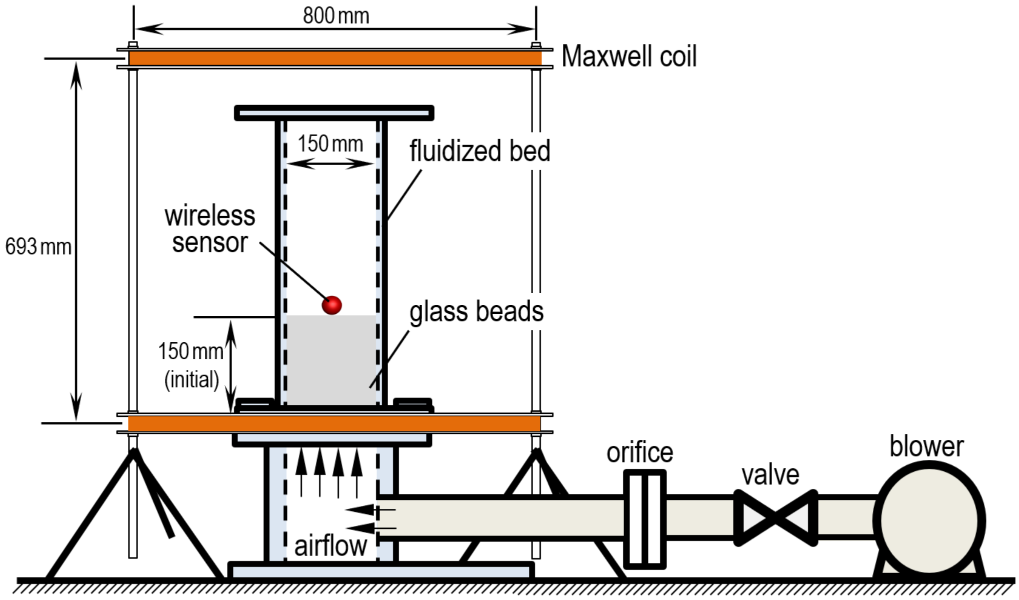

Fig.4 Schematic diagram of experimental system.

high porosity region is permanently observed at the bottom of the bed [23,25]. The apparent density of the fluidized bed ρ_a changes with the air velocity condition, because it depends on the fluidized state. As a rough guide, if the particle bed is gently fluidized (e.g., u_0/u_{mf} is close to 1), the apparent density is approximately ρ_a =1500 kg/m^3.

In the initial state, the media particles (i.e., the glass beads) were put into the experimental vessel with a bed height L = 150 mm and the capsules containing the Lagrangian sensor were placed on the surface of the bed. Then, acquisition of the wireless signals from the Lagrangian sensor was initiated started and the air supplies from the bottom of the experimental apparatus. The wireless measurement was performed for 40–60 seconds.

As mentioned in the Introduction, the float-sink motion of a spherical object in gas-fluidized bed was examined experimentally in our previous study [23]. The previous experiment found that the vertical motion of the spherical object complicatedly depend on the object density and the fluidization state. In particular, an object with a similar density to the apparent density of the fluidized bed exhibits the most complicated float-sink motion. Therefore, we investigated the shape effect on the vertical motion of the object with a similar density to ρ_a in this study. The mass of the object (Lagrangian sensor) was adjusted by putting clay paste and lead pieces into the capsule. The density of all objects was set to be constant as ρ_s=1800 kg/m^3.

3. Results and Discussion

3.1 Float-Sink Motion of Variously-shaped Objects

Figure 5 shows the measurement results of vertical positions and attitude angles of the disk objects ($Ar = 2$ and $Ar = 3$), the sphere, and the cylinders ($Ar = 2$ and $Ar = 3$). Note that the results of attitude angle for the sphere are not shown here because of its isotropic geometry. The results in Fig.5 represent measurements taken over for approximately 30 seconds after the start of fluidization. As mentioned earlier, under the condition of air velocity $u_0/u_{mf} = 4.0$, the fluidized bed expands considerably and therefore the vertical position of the object exceeded the initial layer height of 150 mm at some moments.

As shown in the upper plots of Fig. 5 (a) and (b), the disk-shaped objects periodically moved up and down in the fluidized bed after fluidization. On the other hand, as shown in Fig. 5 (c), the sphere stayed at the bottom of the particle bed for most of the measurement period and occasionally exhibited sudden upward movements. The cylinder-shaped objects shown in Fig. 5 (d) and (e) repeatedly

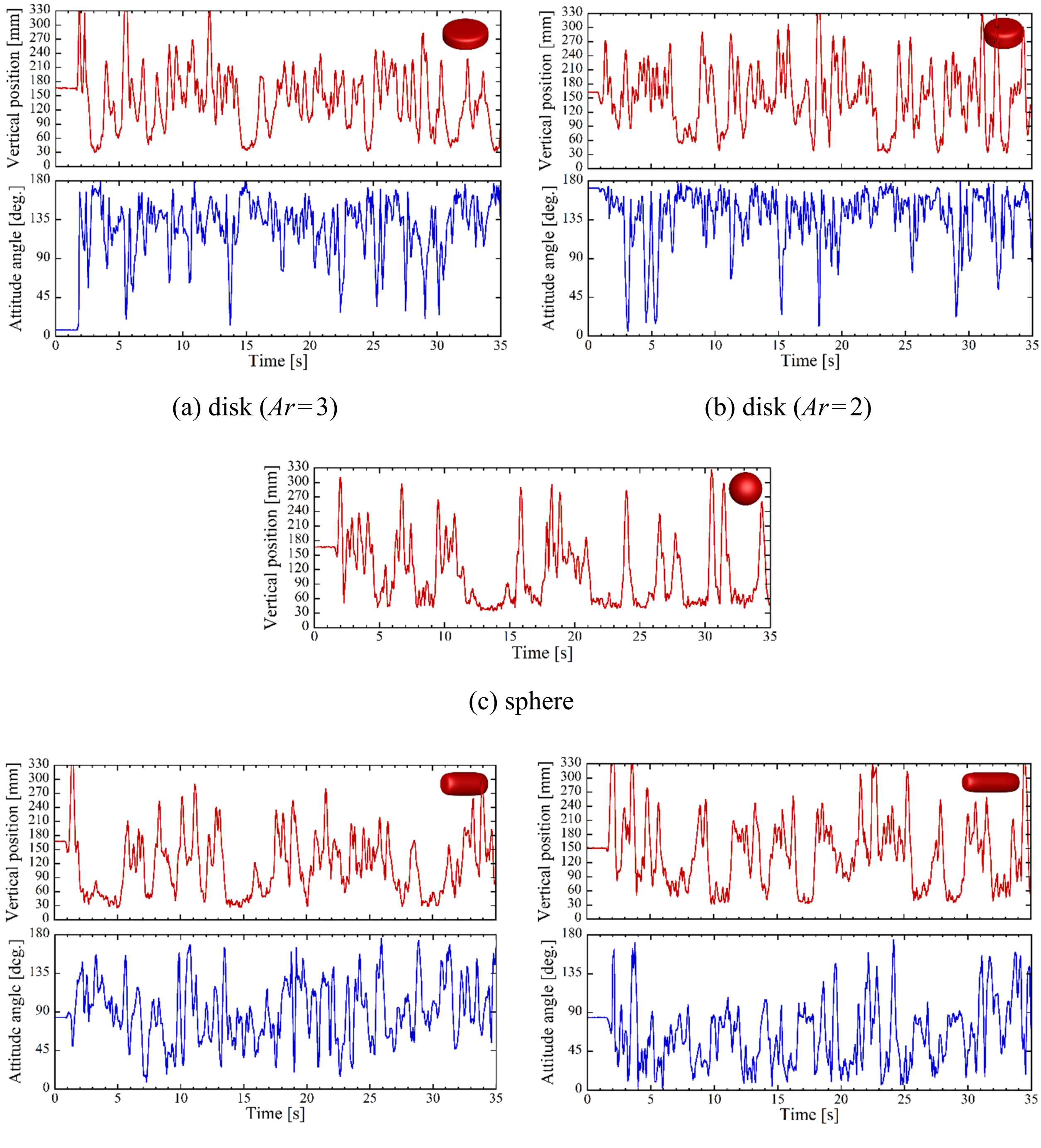

(a) disk (Ar=3) (b) disk (Ar=2)

(c) sphere

(d) cylinder (Ar=2) (e) cylinder (Ar=3)

Fig.5 Experimental results of vertical position and attitude angle of variously-shaped objects for u_0/u_{mf}=4.0 (upper: vertical position, lower: attitude angle). (c) shows only the vertical position.

stagnated at the bottom of the bed and suddenly moved up. As mentioned in the previous section, the volumes of these objects were equal, so the float-sink motion of the objects should be similar when considered in terms of volumetric forces, e.g., buoyancy. Nevertheless, the vertical motion of each object was completely different. These results suggest that the shape of the object greatly influences the float-sink motion.

Figure 6 shows the probability densities of the vertical position of (a) the disk for $Ar=3$, (b) the disk for $Ar=2$, (c) the sphere, (d) the cylinder for $Ar=2$, and (e) the cylinder for $Ar = 3$, for 30 seconds after fluidization, respectively. As mentioned above, the apparent density of the fluidized bed was estimated to be approximately ρ_a =1500 kg/m^3 in this experiment, whereas the object density was ρ_s=1800 kg/m^3. Therefore, assuming an ideal hydrostatic pressure gradient in the fluidized bed,

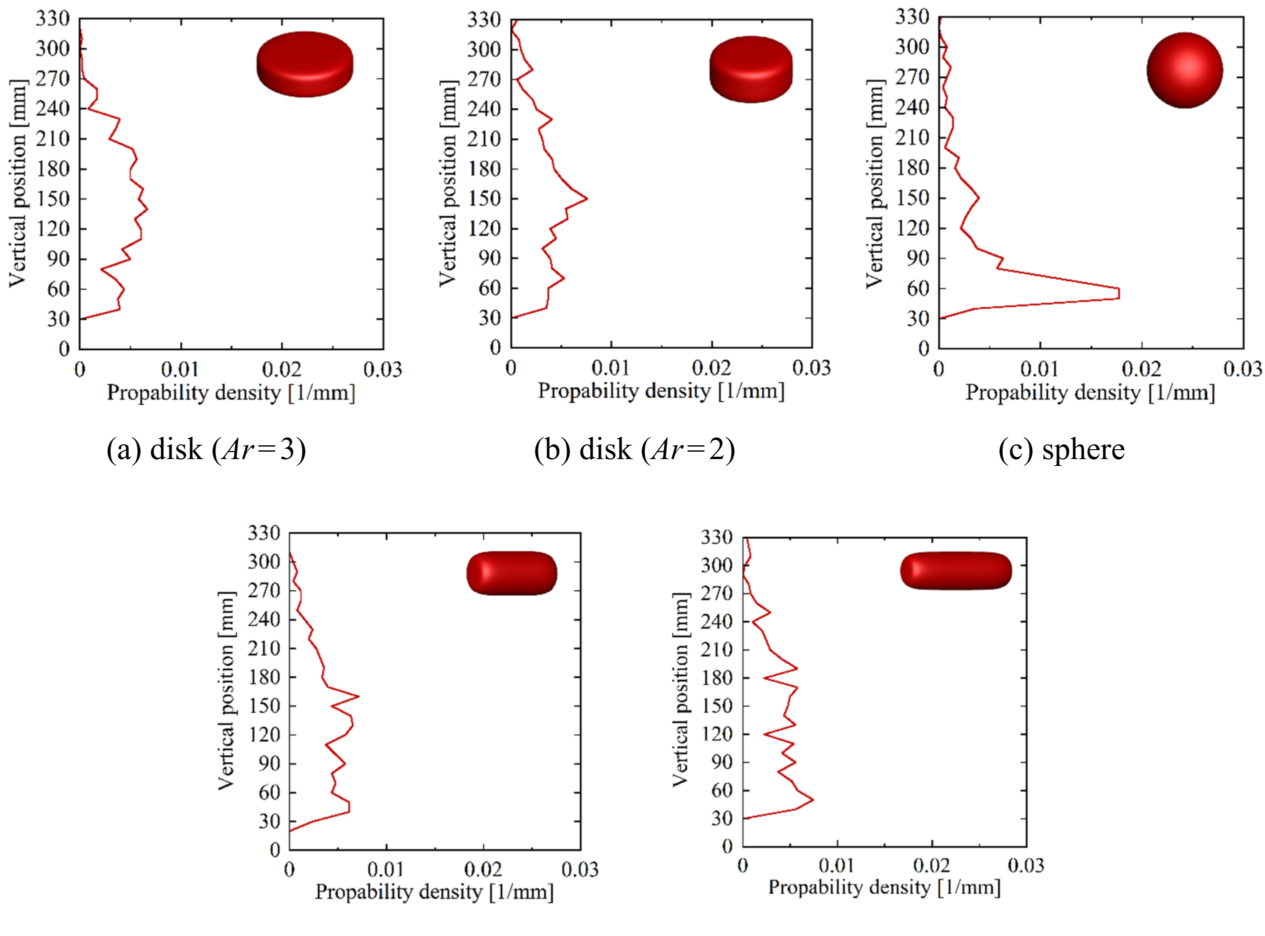

(a) disk (Ar=3) (b) disk (Ar=2) (c) sphere

(d) cylinder (Ar=2) (e) cylinder (Ar=3)

Fig.6 Probability density of vertical position of variously-shaped objects for u_0/u_{mf}=4.0.

the object was expected to settle due to the density difference under these conditions. Fig. 6 shows that the probability density of spherical objects was primarily distributed at the bottom of the fluidized bed, while those of disks and cylinders are widely distributed in vertical direction. Therefore, non-spherical objects tend to float more easily than spherical objects.

As already described in our previous study [25], the probability density profiles of the vertical position of both spherical and non-spherical objects were in quantitative agreement with the results of numerical simulations under the same conditions. However, for the cylinder and disk with a small aspect ratio ($Ar=2$), differences were observed in the probability density depending on the number of trials, while the results for non-spherical objects with a large aspect ratio ($Ar=3$) were reproducible across multiple trials. Thus, in the following, a more detailed discussion is provided with a focus on non-spherical objects with large aspect ratios (e.g., $Ar=3$).

As shown in Fig. 6, the probability densities of the non-spherical objects appear to be almost similar, however, it is found from Fig. 5 that the instantaneous vertical motions of the objects were quite different. That is, the disk-shaped object floated in the fluidized bed for most of the time, but was occasionally stagnant at the bottom of the bed for a few seconds (Fig.5a). In contrast, once the cylindrical object settled to the bottom, it remained there for a relatively long period of time and then repeated the floating motion (Fig.5e). Further discussion of these differences in the observed float-sink motions of non-spherical objects, including consideration of attitude angles, is given in the next section.

3.2 Angular Motion of Cylinder-shaped Object

The attitude of non-spherical objects during the float-sink motion was investigated. Figure 7 shows a close-up view of the measured vertical position and attitude angle of the cylinder-shaped object (*Ar* = 3) shown in Fig.5(e). Fig. 7 shows a period of two seconds (16.2 s–18.2 s) presenting the moment at which the cylinder descended and ascended. When the cylinder descended, the attitude angle was almost 0 deg. and then the angle kept approximately 90 deg. while it stayed at the bottom. When the cylinder ascended again, the angle was again close to 0 deg.. Similar angular motions were observed during other periods (e.g., 6–8 s, 10–12s, 25–27s and 28–30s), i.e., the long axis of the cylinder is heading down during sinking and became parallel after reaching the bottom, and then the long axis is heading upward during rising again. This can be interpreted that the cylinder moved vertically

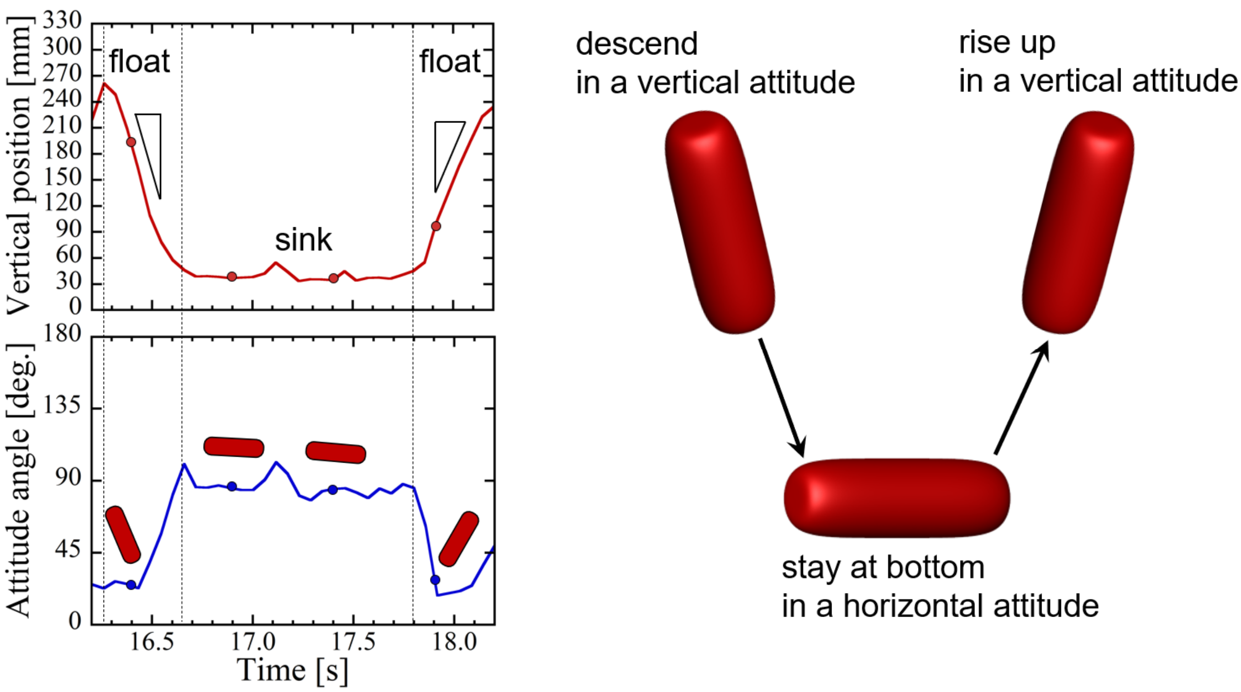

Fig. 7 Schematic of angular motion of cylinder-shaped object.

oriented in the longitudinal direction, but it became trapped in a high void region at the bottom, oriented in horizontal direction (See the right image in Fig.7). In other words, if the cylinder can change its attitude, it may escape from the bottom. On the other hand, because the sphere is isotropic in shape, there is little opportunity for the sphere to escape the high void region at the bottom, compared to the cylinder case.

These features of a cylindrical object can be also seen in the results of numerical analysis reported in the previous study. Figure 8 represents the numerical results of angular motions of cylinder-shaped objects ($Ar = 3$) conducted under the same condition of this experiment [25]. The images in Fig.8

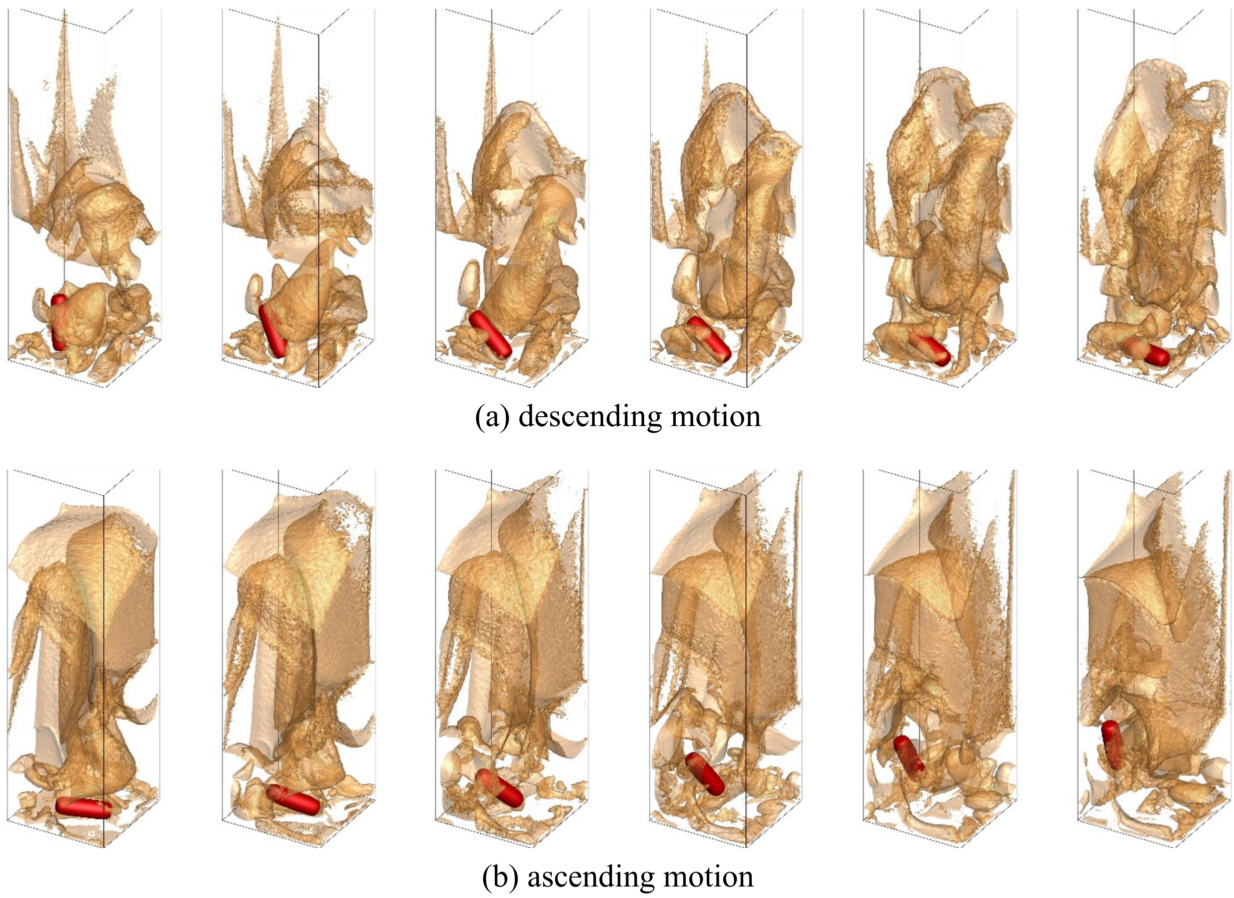

(a) descending motion

(b) ascending motion

Fig.8 Numerical results of angular motion of cylinder-shaped object. The images were produced from the numerical results of Ref.[25] for representing the detailed vertical motion of the cylinder. Time intervals are 0.025 s. for both descending and ascending motions.

were reproduced from the numerical results for representing the detailed angular motion of the cylinder during its ascending or descending motions. Time intervals in each image are 0.025 s for both motions.. The iso-surfaces represent a porosity of media particles ε=0.85. As can be seen in Fig.8, the similar angular motions indicating in Fig.7 were also observed in numerical results.

3.3 Angular Motion of Disk-shaped Object

Figure 9 shows the vertical position and attitude angle of a disk-shaped object (Ar = 3) in a gas-solid fluidized bed. Here we pick up two types of float-sink motion of the disk object. The upper-left figure illustrates a short period (2.5 s–4.5 s) of the moment of rapid vertical motion of the disk. As can be seen, the disk descended at an attitude angle of approximately 90 deg., and remained at the bottom with around 180 deg., and then ascended at approximately 90 deg. again. Similar motions were also observed in other periods (e.g., 24 s–26 s and 33 s–35 s).

However, an additional ascending mode was observed for the disk object. The upper-right figure shows the moment of slow rising mode of the disk (31 s–33 s). When the disk ascended slowly, the attitude angle remained close to 180 deg., i.e., the disk ascended in a mostly horizontal orientation. Note that this mode was also observed in other periods (e.g., 16 s–18 s), although less frequently.

From these results, it appears that there are two primary rising mechanisms for the disk-shaped objects, i.e., rapid rising in a vertical attitude and gentle rising in a horizontal attitude, as shown in the lower image in Fig.9. The similar angular motion can be also seen in the numerical simulation. Figure 10 represents the numerical results of instantaneous angular motion of the disk-shaped object

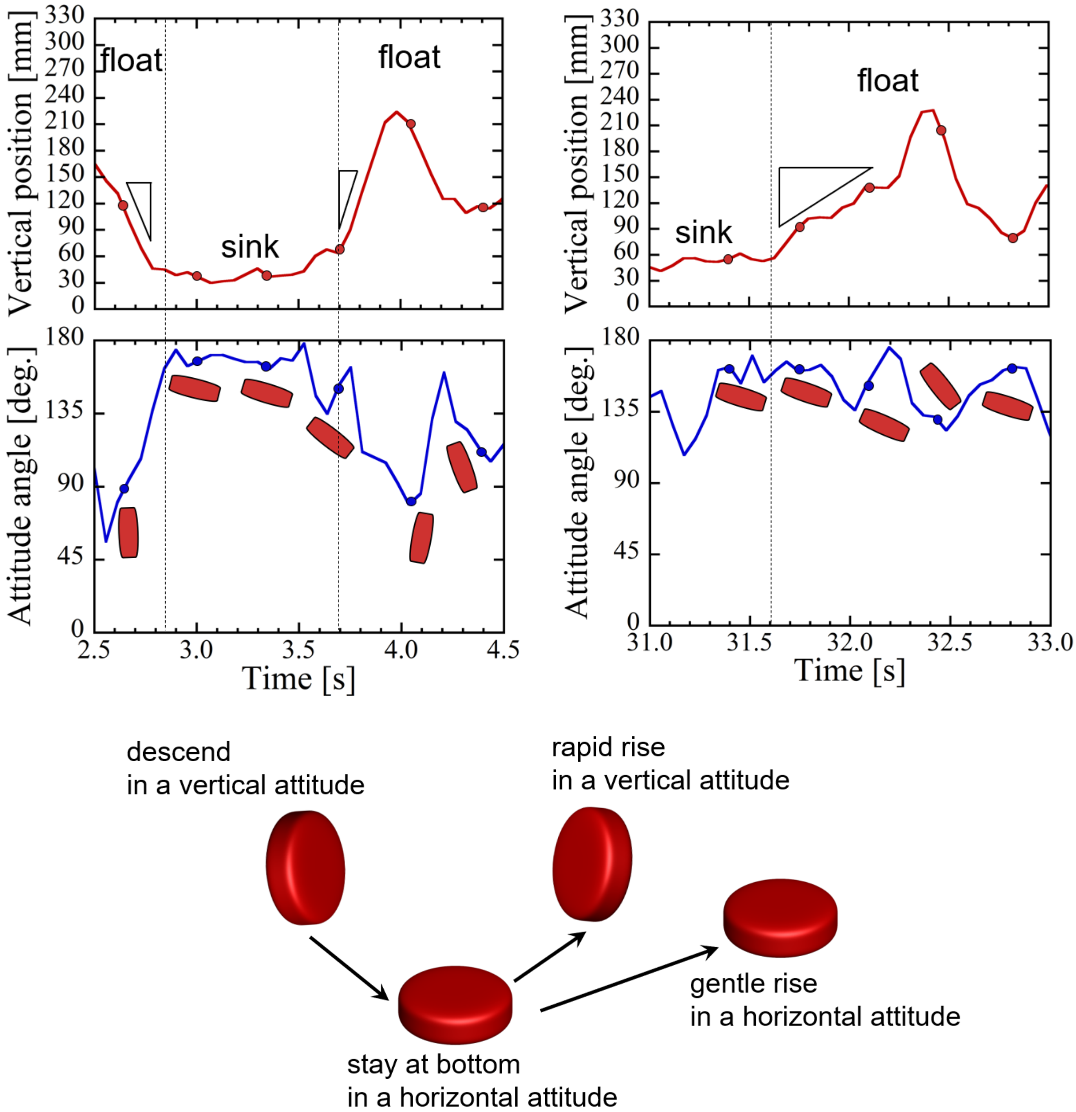

Fig.9 Schematic of angular motion of disk-shaped object

(Ar = 3) under the same conditions of the experiment [25]. The numerical simulation predicted the two rising modes of the disk-shaped objects as mentioned above. The rapid rising in a vertical attitude shown in Fig.10 (a) may occur by the similar mechanism to that of the cylinder discussed in the previous section. The mechanism of gentle rising in a horizontal attitude, which is shown in Fig.10 (b), is not sure at the present stage, however, it is inferred that the disk ascends keeping a horizontal attitude to follow the local upward motion of the media particles, since the projected area of the disk-

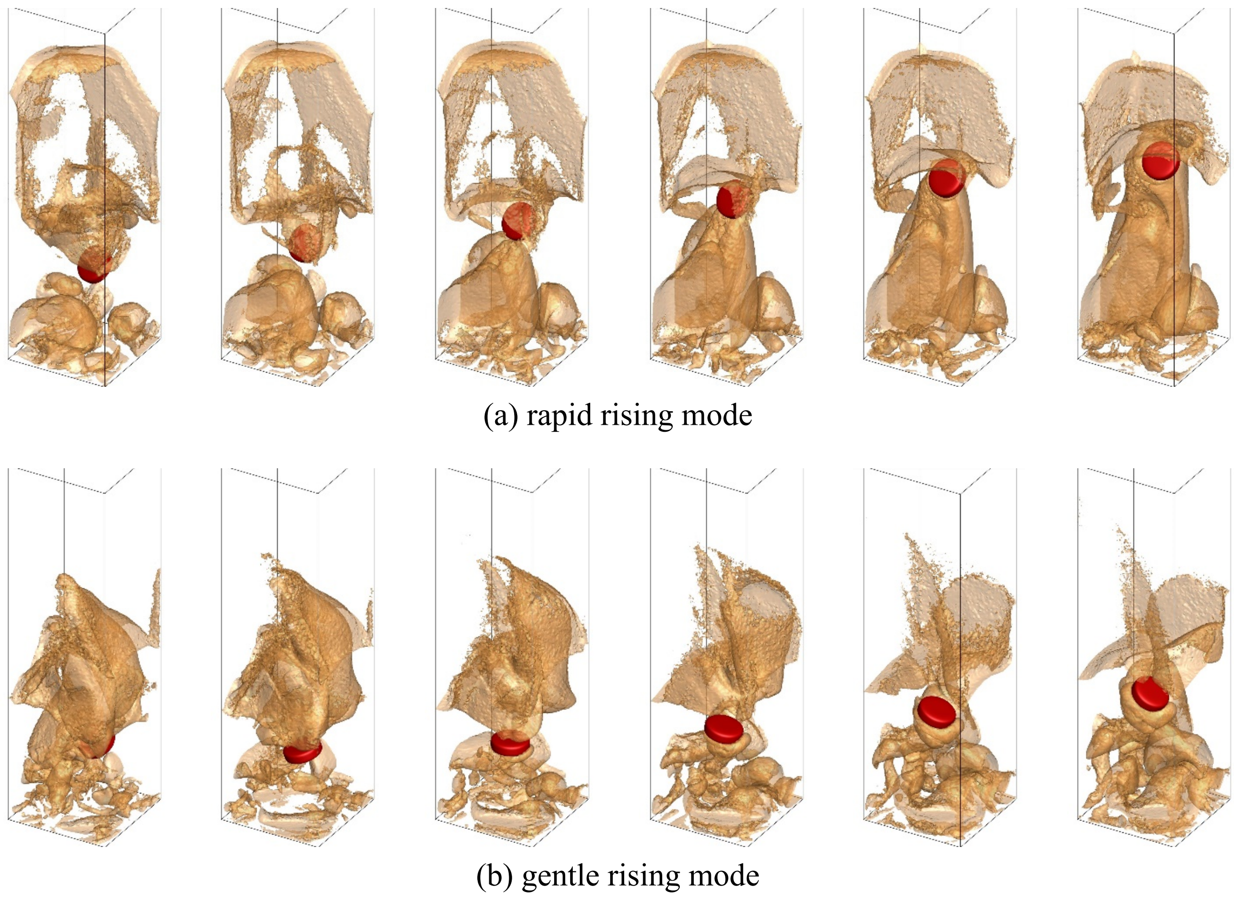

Fig.10 Numerical results of angular motion of disk-shaped object. The images were produced from the numerical results of Ref.[25]. Time intervals are 0.025 s for both modes.

shaped object is larger than the sphere and cylinder-shaped ones.

Conclusions

The float-sink motions of coarse objects of various shapes in a gas-solid fluidized bed were investigated experimentally. A wireless sensor system that can measure the vertical force and attitude angle simultaneously was used to examine the object motion in a fluidized bed, which cannot be observed from the outside. The outer shell of the sensor system was designed by the super-ellipsoid model and fabricated by a 3D printer. In our experiments, the spherical and non-spherical objects were adjusted to the same mass and volume, so that their density was close to the apparent density of the fluidized bed.

The experimental results demonstrated that the float-sink motion of the objects in the gas-solid fluidized bed varied greatly depending on the shape of the object. These results were in contrast to buoyant motion in water. The non-spherical objects, such as cylinders and disks, tended to float more than a spherical object of equal volume. These tendencies were similar to the results of numerical analyses performed under the same conditions in the previous study [25].

The objects immersed in the fluidized bed float and sink periodically, but the frequency and interval time varied depending on the object shape. Such differences in the unsteady motions were revealed by examining the angular motion of the objects. The non-spherical objects such as disks and cylinders sank vertically along these longitudinal directions, and then remained at the bottom of the fluidized bed with their attitude turned sideways. Subsequently, the change in the fluidized state of the media particles triggered them to start moving upward. These characteristic motions of non-spherical objects were rarely observed in spherical objects.

In terms of engineering applications, the float-sink motions of variously-shaped objects shown here, which are in contrast to those in water, are important in terms of the dry density separation utilized in the fluidized bed. Based on our findings, the separation efficiency is likely influenced by the shape of the object, particularly under density conditions close to the apparent density of the fluidized bed (i.e., the float-sink boundary).

Conflict of Interest

The authors declare that there is no conflict of interest.

Acknowledgment

A part of this study was supported by JSPS KAKENHI Grant Number JP21H03646.

References

[1] Kunii, D. and Levenspiel, O., *Fluidization Engineering, 2nd ed.*, (1991) Butterworth-Heinemann, Boston.

[2] Soria-Verdugo, A., Garcia-Gutierrez, L. M., Garcia-Hernando, N. and Ruiz-Rivas, U., Buoyancy effects on objects moving in a bubbling fluidized bed, *Chem. Eng. Sci.,* 266 (2011) 2833–2841.

[3] Fotovat F., Chaouki J. and Bergthorson, J., Distribution of large biomass particles in a sand-biomass fluidized bed: experiments and modeling, *AIChE J.,* 60 (2014) 869–880.

[4] Chen. X., Zhong, W. and Heindel, T. J., Orientation of cylindrical particles in a fluidized bed based on stereo X-ray particle tracking velocimetry (XPTV), *Chem. Eng. Sci.,* 203 (2019) 104–112.

[5] Chen. X., Zhong, W. and Heindel, T. J., Using stereo XPTV to determine cylindrical particle distribution and velocity in a binary fluidized bed, *AIChE J.,* 65 (2019) 520–535.

[6] Müller, D., Plankenbühler, T. and Karl, J., A methodology for measuring the heat release efficiency in bubbling fluidised bed combustors, *Energies*, 13 (2020) 2420.

[7] Iannello, S., Bond, Z., Sebastiani, A., Errigo, M. and Materazzi, M., Axial segregation behaviour of a reacting biomass particle in fluidized bed reactors: experimental results and model validation, *Fuel*, 338 (2023) 127234.

[8] Oshitani, J., Kajimoto, S., Yoshida, M., Franks, G. V., Kubo, Y. and Nakatsukasa, S., Continuous float–sink density separation of lump iron ore using a dry sand fluidized bed dense medium, *Adv. Pow. Tech.,* 24 (2013) 468–472.

[9] Oshitani, J., Sasaki, T., Tsuji, T., Higashida, K. and Chan, D. Y. C., Anomalous sinking of spheres due to local fluidization of apparently fixed powder beds, *Phys. Rev. Lett.*, 116 (2016) 068001.

[10] Tsuji, T., Penn, A., Hattori, T., Pruessmann, K. P., Müller, C.R., Oshitani, J., Washino, K. and Tanaka, T., Mechanism of anomalous sinking of an intruder in a granular packing close to incipient fluidization, *Phys. Rev. Fluids*, 6 (2021) 064305.

[11] Penn, A., Tsuji, T., Brunner, D. O., Boyce, C. M., Pruessmann, K. P. and Müller, C. R., Real-time probing of granular dynamics with magnetic resonance**,** *Sci. Adv.*, 3 (2017) e1701879.

[12] Fotovat, F., Ansart, R., Hemati, M., Simonin, O. and Chaouki, J., Sand-assisted fluidization of large cylindrical and spherical biomass particles: Experiments and simulation, *Chem. Eng. Sci.*, 126 (2015) 543–559.

[13] Köhler, A., Rasch, A., Pallarés and Johnsson, F., Experimental characterization of axial fuel mixing in fluidized beds by magnetic particle tracking, *Powder Technol.*, 316 (2017) 492–499.

[14] Che, H., Werner, D., Seville, J., Wheldon, T. K. and Windows-Yule, K., Evaluation of coarse-grained CFD-DEM models with the validation of PEPT measurements, *Particuology,* 82 (2023) 48–63.

[15] Wadke, P. M., Hounslow, M. J. and Salman A. D., The 'smart' sphere, experimental results, *Chem. Eng. Res. Des.*, 83 (2005) 1298–1302.

[16] Shew, W. L., Gasteuil, Y., Gibert, M., Metz, P. and Pinton, J.-F., Instrumented tracer for Lagrangian measurements in Rayleigh-Bénard convection, *Rev. Sci. Instrum.*, 78 (2007) 065105.

[17] Gasteuil, Y., Shew, W. L., Gibert, M., Chillá, F., Castaing, B. and Pinton, J.-F., Lagrangian temperature, velocity, and local heat flux measurement in Rayleigh-Bénard convection, *Phys. Rev. Lett.*, 99 (2007) 234302.

[18] Thiele, S., Silva, J.D. and Hampel, U., Autonomous sensor particle for parameter tracking in large vessels, *Meas. Sci. Technol.,* 21 (2010) 085201.

[19] Harada, S., Kobayashi, Y., Sawano, T. and Noguchi, E., Direct measurement of fluid force on a particle in liquid by telemetry system, *Int. J. Multiphase Flow*, 37 (2011) 898–905.

[20] Sánchez-Colina, G., Alonso-Llanes, L., Martínez, E., Batista-Leyva, A. J., Clement, C., Fliedner, C., Toussaint, R. and Altshuler, E., Note: "Lock-in accelerometry" to follow sink dynamics in shaken granular matter, *Rev. Sci. Instrum.*, 85 (2014) 126101.

[21] Bisgaard, J., Muldbak, M., Cornelissen, S., Tajsoleman, T. Huusom, J. K., Rasmussen. T. and Gernaey, K. V., Flow-following sensor devices: a tool for bridging data and model predictions in large-scale fermentations, *Comp. Str. Biotech. J.*, 18 (2020) 2908–2919.

[22] Higashida, K., Rai, K., Yoshimori, W., Ikegai, T., Tsuji, T., Harada, S., Oshitani, J. and Tanaka, T., Dynamic vertical forces working on a large object floating in gas-fluidized bed: discrete particle simulation and Lagrangian measurement**,** *Chem. Eng. Sci.*, 151, (2016) 105–115.

[23] Yoshimori, W., Ikegai, T., Uemoto, K., Narita, S., Harada, S., Oshitani, J., Tsuji, T., Kajiwara, H. and Matsuoka, K., Non-invasive measurement of floating-sinking motion of a large object in a gas-solid fluidized bed, *Gran. Matt.*, 21 (2019) 1–11.

[24] Tsuji, T., Higashida, K., Okuyama, Y. and Tanaka, T. Fictitious particle method: a numerical model for flows including dense solids with large size difference, *AIChE J.,* 60 (2014) 1606–1620.

[25] Tsuji, T., Sakamoto, Y., Harada, S., Uemoto, K., Oshitani, J., Washino, K., Tanaka, T., Kajiwara, H. and Matsuoka, K., FPM-SE: a numerical model for dense gas-solid flows with large non-spherical object, *Chem. Eng. Sci.*, 264 (2022) 118149.

[26] Honda, Y., Saito, S., Anzai, T., Harada, S., Tsuji, T., Washino, K., Oshitani, J., Kajiwara, H. and Matsuoka, K., Experimental verification of the Brinkman equation around objects with various shapes in gas–solid stationary and fluidized beds, *Int. J. Multiphase Flow*, 160 (2023) 104359.

[27] Wellmann, C., Lillie, C. and Wriggers, P., A contact detection algorithm for super ellipsoids based on the common-normal concept, *Eng. Comput.*, 25 (2008) 432–442.

[28] Geldart, D., Types of gas fluidization, *Powder Technol.*, 7 (1973) 285–292.